High-accuracy optical clocks based on group-16-like highly charged ions

Saleh O. Allehabi, S. M. Brewer, V. A. Dzuba, V. V. Flambaum, and K. Beloy

High-accuracy optical clocks based on group 16-like highly charged ions

Saleh O. Allehabi,[1,2] S. M. Brewer,[3] V. A. Dzuba,[1] V. V. Flambaum,[1] and K. Beloy[4]

[1]*School of Physics, University of New South Wales, Sydney 2052, Australia*
[2]*Department of Physics, Faculty of Science, Islamic University of Madinah, Madina 42351, KSA*
[3]*Department of Physics, Colorado State University, Fort Collins, Colorado 80523, USA*
[4]*National Institute of Standards and Technology, Boulder, Colorado 80305, USA*
(Dated: September 13, 2022)

We identify laser-accessible transitions in group 16-like highly charged ions as candidates for high-accuracy optical clocks, including S-, Se-, and Te-like systems. For this class of ions, the ground ^3P_J fine structure manifold exhibits irregular (nonmonotonic in J) energy ordering for large enough ionization degree. We consider the $|^3P_2\rangle \longleftrightarrow |^3P_0\rangle$ (ground to first-excited state) electric quadrupole transition, performing relativistic many-body calculations of several atomic properties important for optical clock development. All ions discussed are suitable for production in small-scale ion sources and lend themselves to sympathetic cooling and quantum-logic readout with singly charged ions.

I. INTRODUCTION

The performance of optical clocks has improved rapidly over the last few decades [1]. This has led to improvements in frequency metrology as well as tests of fundamental physics using atomic clocks [2]. The highest performance optical clocks are currently based on ensembles of neutral atoms trapped in optical lattices or singly charged ions stored in electromagnetic traps [3–6]. However, in recent years, several clocks based on highly charged ions (HCIs) have been proposed as both improved optical frequency standards and as systems with enhanced sensitivity to possible new physics [7–9] (see also Ref. [10] and references therein). Optical clocks based on HCIs provide several systematic advantages over current optical clocks including reduced blackbody radiation (BBR), Zeeman, and electric quadrupole shifts [10, 11]. Here, we identify group 16-like HCIs as optical clock candidates. For this class of ions, the ground ^3P_J fine structure manifold exhibits irregular (nonmonotonic in J) energy ordering for large enough ionization degree, with the $^3P_1$ state lying above the $^3P_2$ (ground) and $^3P_0$ (first-excited) states. Given this irregular ordering, the $^3P_0$ excited state lacks a magnetic dipole ($M1$) decay channel, resulting in a relatively long lifetime and making the $|^3P_2\rangle \longleftrightarrow |^3P_0\rangle$ electric quadrupole ($E2$) transition a viable clock transition. This irregular energy ordering is illustrated in Fig. 1. Due to the high nuclear charge, the ordering is irregular for Te-like systems beginning with neutral tellurium. In the case of O-, S-, and Se-like systems, the ionization degree must be increased before the irregular ordering is observed. Specifically, for O-like ions, the irregular ordering is not observed until Mn^{17+}. For this system, the clock transition wavelength (≈ 150 nm [12, 13]) is outside the range of current clock lasers. The S-, Se-, and Te-like systems offer more favorable clock transition wavelengths. In the present work, we perform relativistic many-body calculations of relevant properties for optical clock development. While we present results only for select S-, Se-, and Te-like systems, other group 16-like systems not explicitly considered may

also be of interest.

The present work is a broader study of the group 16-like systems started in our previous work with just Ba^{4+} [17]. We include Ba^{4+} in the list of ions considered here. Broadly speaking, similar computational techniques are used here as in Ref. [17]. The results of Ref. [17] are reproduced with only small deviations, with two exceptions. First, a small clerical error is corrected, giving a second order Zeeman shift that is a factor of two larger. The essential conclusion that this shift is negligible remains valid. Second, an improved method is used to calculate the scalar differential polarizability $\Delta\alpha$, which predicts a much larger degree of cancellation between the clock state polarizabilities. While the revised value of $\Delta\alpha$ does not support cancellation between the trap-induced Stark and micromotion time-dilation shifts (by operating at a magic rf trap drive frequency [18]), it does offer highly suppressed Stark shifts, including the BBR shift. We find similar cancellation between the clock state polarzbilities for the other group 16-like systems, resulting in similarly small $\Delta\alpha$.

In the present work, we focus on the isotopes with zero nuclear spin to avoid complications caused by the hyperfine structure (hfs). In particular, the second-order Zeeman shift is enhanced in isotopes with hfs, by small hfs energy intervals. In contrast, the second-order Zeeman shift is small and can be neglected in spin-zero isotopes.

II. METHOD

A. Calculation of energy levels

The calculations are carried out using a combination of the configuration interaction (CI) technique with the linearized single-doublecoupled-cluster (SD) method, as described in Ref. [19]. The combined method (CI+SD) has been demonstrated to be efficient and very precise for systems with several valence electrons. With the SD technique, it is possible to accurately determine the core-valence and core-core electron correlations, while the CI
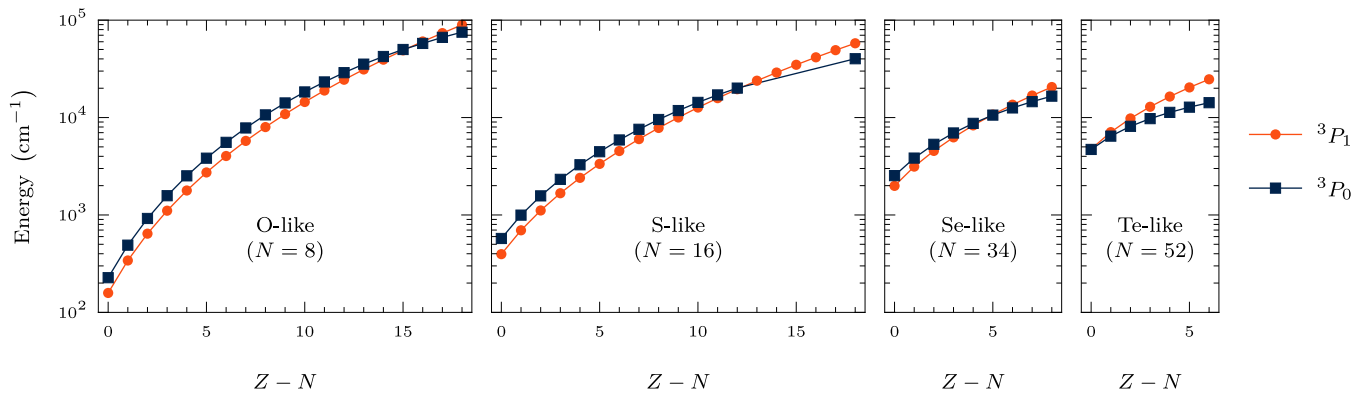
FIG. 1. Experimental energies for group 16-like atomic systems. For each system, the lowest-lying electronic states are part of a ^3P_J fine structure manifold, with the $^3P_2$ ground state taken to have zero energy. Energies of the $^3P_1$ and $^3P_0$ states are plotted versus ionization degree $Z - N$ for the isoelectronic sequences, where Z and N denote the number of protons and electrons, respectively. For the O, S, and Se isoelectronic sequences, the ^3P_J energy ordering transitions from regular ordering (monotonic in J) at low ionization degree to irregular ordering at high ionization degree. For the Te isoelectronic sequence, the ordering is irregular already for the neutral Te system. For the systems with irregular energy ordering, the $^3P_0$ state lacks an $M1$ decay channel. Energies are from the NIST Atomic Spectra Database [12] and Refs. [14–16]. The curves are interpolating functions intended to guide the eye.

method takes the valence-valence correlations into account. Our calculations are done using the V^{N-M} approximation [19], where N is the total number of electrons and M is the number of valence electrons. For all atomic systems considered (see, e.g., Table I), the calculations begin with the relativistic Hartree-Fock (RHF) method for a closed-shell core, which removes all valence electrons. We treat all systems as $M = 6$ valence systems, except for Te and Sr^{22+}, which are treated as $M = 4$ valence systems; this is because NIST data [12] indicate that Te and Sr^{22+} have no low-lying states with the excitations from the $5s$ and $3s$ subshells, respectively. Therefore, it is reasonable to treat $5s$ electrons in Te and $3s$ electrons in Sr^{22+} as core electrons. The RHF Hamiltonian has the following form:

$$\hat{H}^{\mathrm{RHF}} = c\boldsymbol{\alpha} \cdot \mathbf{p} + (\beta - 1)mc^2 + V_{\mathrm{nuc}}(r) + V_{\mathrm{core}}(r), \quad (1)$$

where c is the speed of light, $\boldsymbol{\alpha}$ and β are the Dirac matrices, $\boldsymbol{p}$ is the electron momentum, m is the electron mass, V_{nuc} is the nuclear potential obtained by integrating the Fermi distribution of the nuclear charge density, and $V_{\mathrm{core}}(r)$ is the self-consistent RHF potential created by the electrons of the closed-shell core.

Following the completion of the self-consistent procedure for the core, the B-spline technique [20, 21] is used to develop a complete set of single-electron wave functions. Based on B-splines, one can make linear combinations of basis states, which are eigenstates of the RHF Hamiltonian. The basis set is built up of 40 B-splines of order 9 in a box that has a radius $R_{\mathrm{max}} = 40a_B$, where a_B is the Bohr radius, with the orbital angular momentum $0 \le l \le 6$. There are two types of basis states: core states and valence states. Core states are used to calculate the effective potential of the core. Valence states are used as a basis for the SD equations and for obtaining

the many-electron states required for the CI calculations.

In the process of solving the SD equations for the core and valence states, we generate correlation operators Σ_1 and Σ_2 [19, 22, 23]. Σ_1 is the correlation interaction between a particular valence electron and the core, and accordingly, one-body part $\hat{h}_1$ can be described as follows

$$\hat{h}_1 = \hat{H}^{\mathrm{RHF}} + \Sigma_1. \quad (2)$$

Σ_2 represents the screening of the Coulomb interaction between a pair of valence electrons; hence, the two-body Coulomb interaction operator, $\hat{h}_2$, is modified so as to include the two-body part of the core-valence interaction as follows (we use Gaussian electromagnetic expressions, e is electron charge)

$$\hat{h}_2 = \frac{e^2}{|r_i - r_j|} + \Sigma_2. \quad (3)$$

Whenever there are more than one valence electron above the closed-shell core, these Σ operators can be used in the subsequent CI calculations to account for the core-valence and core-core correlations. By solving the SD equations for external states, the single-electron energies of an atom or ion with one valence electron can also be obtained. However, we note that there are slight differences between the SD equations used for this purpose and those to be used for CI calculations. In this case, one term in the SD equations needs to be eliminated because its contribution is accounted for by the CI calculations (refer to Ref. [19]). This contribution is relatively small; therefore, differences in the SD equations can be ignored.

In the CI approach, we build the effective CI+SD Hamiltonian for many valence electrons as a sum of one- and two-electron parts with the addition of Σ_1 and Σ_2 operators in order to account for the correlation between

core and valence electrons,

$$\hat{H}^{\text{eff}} = \sum_{i=1}^{M} \left(\hat{H}^{\text{RHF}} + \Sigma_1 \right)_i + \sum_{i<j}^{M} \left(\frac{e^2}{|r_i - r_j|} + \Sigma_{2ij} \right)(4)$$

where i and j enumerate valence electrons.

It is well-recognized that increasing the number of valence electrons exponentially increases the size of the CI matrix. Our present work has up to six valence electrons, which leads to an extremely large CI matrix. In order to deal with a matrix of this magnitude, it would require considerable computational power. However, the size of the CI matrix can be decreased by orders of magnitude at the expense of some accuracy. In order to accomplish this, we use the recently developed version of the CI method called the CIPT method [24]. The method combines CI with perturbation theory (PT) and is used to ignore the off-diagonal matrix elements between high-energy states in the CI matrix. This step is justified because the high-energy states provide only a minimal correction to the wave function.

The wave function for valence electrons is presented as an expansion over single-determinant basis states, which is divided in two parts,

$$\Psi \left(r_1, \ldots, r_M \right) = \sum_{i=1}^{N_{\text{eff}}} c_i \Phi_i \left(r_1, \ldots, r_M \right)$$
$$+ \sum_{i=N_{\text{eff}}+1}^{N_{\text{total}}} c_i \Phi_i \left(r_1, \ldots, r_M \right). \tag{5}$$

Here c_i are the expansion coefficients and Φ_i are single-determinant many-electron basis functions. The first part of the wave function represents a small number of low-energy terms that contribute a great deal to the CI valence wave function ($1 \leqslant i \leqslant N_{\text{eff}}$, where N_{eff} is the number of low-energy basis states), while the second part represents a large number of high-energy states that introduce minor corrections to the valence wave function ($N_{\text{eff}} < i \leqslant N_{\text{total}}$, where N_{total} is the total number of the basis states). Consequently, this allows us to truncate the CI Hamiltonian by ignoring the off-diagonal matrix elements between terms in the second summation in Eq. (5) ($\langle i | H^{\text{eff}} | h \rangle = 0$ for $N_{\text{eff}} < i, h \leqslant N_{\text{total}}$), which in turn reduces computation time with a negligible loss in precision.

The matrix elements between low-energy states i and g are corrected by the following formula similar to the second-order perturbative correction to the energy

$$\langle i | H^{\text{eff}} | g \rangle \rightarrow \langle i | H^{\text{eff}} | g \rangle + \sum_k \frac{\langle i | H^{\text{eff}} | k \rangle \langle k | H^{\text{eff}} | g \rangle}{E - E_k}. \tag{6}$$

Here, $i, g \leqslant N_{\text{eff}}, N_{\text{eff}} < k \leqslant N_{\text{total}}$, E is the energy of the state of interest, and E_k denotes the diagonal matrix element for high-energy states, $E_k = \langle k | H^{\text{eff}} | k \rangle$. The summation in (6) runs over all high-energy states.

Note that neglecting off-diagonal matrix elements between highly excited states corresponds to neglecting the third-order contribution

$$\delta E_{ig}^{(3)} = \sum_{k,l} \frac{\langle i | H^{\text{eff}} | k \rangle \langle k | H^{\text{eff}} | l \rangle \langle l | H^{\text{eff}} | g \rangle}{(E - E_k)(E - E_l)}. \tag{7}$$

This contribution is supressed by large energy denominators. Neglecting the third-order corrections over the second-order corrections cannot cause any false contributions to the spin-orbit splitting or break the symmetry of the CI Hamiltonian.

The problem of finding the wave function and corresponding energy can be reduced to a modified CI matrix eigenvalue equation $\hat{H}^{\text{eff}}$ [Eq. (4)] with size N_{eff}

$$\left(\hat{H}^{\text{eff}} - EI \right) X = 0, \tag{8}$$

where I is the identity matrix and X is the vector $\{c_1, \ldots, c_{N_{\text{eff}}}\}$. Note that for accurate solution the energy parameter E must be the same in Eqs. (6) and (8). Since this energy is not known in advance, the equations (6) and (8) are solved by iterations. The starting point for the iterations can be, e.g. the solution of (8) with the matrix (6) without the second-order corrections. A more comprehensive description of this technique is given in Ref. [24].

B. Calculation of transition amplitudes and lifetimes

The method we use for computing transition amplitudes is based on the time-dependent Hartree-Fock (TDHF) method [25], which is the same as the well-known random phase approximation (RPA). The RPA equations are defined as

$$\left(\hat{H}^{\text{RHF}} - \epsilon_c \right) \delta\psi_c = - \left(\hat{f} + \delta V_{\text{core}}^f \right) \psi_c, \tag{9}$$

where the operator $\hat{f}$ refers to an external field. The index c denotes single-electron states, ψ_c is a single electron wave function with corresponding energy ϵ_c, $\delta\psi_c$ is a correction to the wave function due to the external field, and δV_{core}^f is the correction to the self-consistent RHF potential caused by the amendment of all core states in the external field. For all states in the core, the RPA equations (9) are solved self-consistently. The transition amplitudes are found by calculating matrix elements between states a and b using the formula

$$A_{ab} = \left\langle b \left| \hat{f} + \delta V_{\text{core}}^f \right| a \right\rangle. \tag{10}$$

Here, $|a\rangle$ and $|b\rangle$ are the many-electron wave functions calculated with the method described above. These wave functions are given by Eq. (5). In the present work, only

the rates of $E2$ transitions are taken into account. The rates are computed as follows (in atomic units)

$$T_{ab} = \frac{1}{15} (\alpha \omega_{ab})^5 \frac{A_{ab}^2}{2J_b + 1}, \tag{11}$$

where α is the fine structure constant ($\alpha \approx \frac{1}{137}$), ω_{ab} is the frequency of the transition, J_b is the total angular momentum of the upper state b, and A_{ab} represents the transition amplitude (reduced matrix element) of the $E2$ operator. The lifetimes of each excited state b, τ_b, expressed in seconds, are given as

$$\tau_b = 2.4189 \times 10^{-17} \bigg/ \sum_a T_{ab} \tag{12}$$

where the summation runs over all possible transitions to lower states a.

III. RESULTS

A. Energy levels, transition amplitudes, and lifetimes of the systems

Table I presents the calculated energy levels of the systems and compares them to the results of previous work; note that all earlier data presented in the table are either experimental or semi-empirical, except for the value for Cd^{14+}, which has been calculated. The calculated energies are in good agreement with experiment, within a few percent. In Table I, we also present the $E2$ amplitudes and corresponding decay rates for excited clock states decaying to the ground state. The rates are in good agreement with previous studies. The rates and lifetimes of the excited clock states were calculated using calculated amplitudes and experimental energies.

B. Ionization potential, Landé g-factors, and electric quadrupole moments

Table II presents the results of the calculated ionization potential (IP) of all atomic systems. The ionization potential (IP) of a system can be calculated as a difference in the ground state energy between the system of interest (E^M) and the following ion (E^{M-1}), IP = $E^{M-1} - E^M$. The results of our calculations are compared with data compiled by NIST. With the exception of the first two systems, the NIST data have large uncertainties ranging from 6800 cm^{-1} to 22000 cm^{-1}. Within these uncertainties, our calculations agree with the NIST data. In Table II, we also present the calculated values of the Landé g-factors for the ground states of all systems. The g-factors are calculated as expectation values of the $M1$ operator.

Electric quadrupole shifts are known to be caused by an interaction between the quadrupole moment of an atomic state and an external electric-field gradient, and in the Hamiltonian, the corresponding term is given as [31]

$$H_{\mathcal{Q}} = \sum_{q=1}^{-1} (-1)^q \nabla \mathcal{E}_q^{(2)} \hat{\Theta}_{-q}. \tag{13}$$

Here, the tensor $\nabla \mathcal{E}_q^{(2)}$ represents the external electric field gradient at the atom's position, and $\hat{\Theta}_q$ describes the electric-quadrupole operator for the atom. It is the same as for the $E2$ transitions, $\hat{\Theta}_q = r^2 C_q^{(2)}$, where $C_q^{(2)}$ is the normalized spherical function and q indicates the operator component. The electric quadrupole moment, Θ, is defined as the expectation value of $\hat{\Theta}_0$ for the extended state

$$\Theta = \left\langle nJJ \left| \hat{\Theta}_0 \right| nJJ \right\rangle$$
$$= \left\langle nJ \| \hat{\Theta} \| nJ \right\rangle \sqrt{\frac{J(2J-1)}{(2J+3)(2J+1)(J+1)}}, \tag{14}$$

where $\left\langle nJ \| \hat{\Theta} \| nJ \right\rangle$ indicates the reduced matrix element of the electric quadrupole operator. We compute the values of Θ using the CI+SD and RPA methods described in the previous section. The results are presented in Table II. Note that the excited clock states of all atomic systems have $\Theta = 0$ since the total angular momentum J is zero. Some of these atomic systems have been investigated before. In our early work [32] a different approach was used leading to quadrupole moments $Q(\text{Te}) = -2.58$ a.u. and $Q(\text{Xe}^{2+}) = -1.17$ a.u. It should be noted that in this earlier work [32], the electric quadrupole moment Q is defined in a way which differs from our definition by a factor of 2, so that $\Theta = Q/2$. Taking this into account, the results for the two calculations are in good agreement.

C. Polarizabilities, blackbody radiation shifts, and second-order Zeeman shifts

The scalar polarizability $\alpha_v(0)$ of an atomic system in state v is given by a sum over a complete set of excited states n connected to state v by the electric dipole ($E1$) reduced matrix elements (we use atomic units)

$$\alpha_v(0) = \frac{2}{3(2J_v + 1)} \sum_n \frac{A_{vn}^2}{\omega_{vn}}, \tag{15}$$

where J_v is the total angular momentum of state v and ω_{vn} is the frequency of the transition. Notations v and n refer to many-electron atomic states. For the calculations of the polarizabilities of clock states, we apply the technique developed in Ref. [33] for atoms or ions with open shells. The method relies on Eq. (15) and the Dalgarno-Lewis approach [34], which reduces the summation in

TABLE I. Excitation energies (E), wavelength transitions (λ), $E2$ amplitudes (A), decay rates (T), and lifetimes (τ) for the excited clock states. Note that for calculating λ, the experimental energies (where available) have been used.

System	State	E [cm^{-1}] Present	E [cm^{-1}] Other	λ [nm]	A [a.u] Present	T [s^{-1}] Present	T [s^{-1}] Other cal.	τ [s] Present
		Te-like systems						
Te	$5p^4\ ^3P_0$	4630	4706[a]	2124.9	-5.483	0.0078	0.0073[f], 0.0097[g]	128.21
Xe^{2+}	$5s^25p^4\ ^3P_0$	8515	8130[a]	1230.0	-3.163	0.0398	0.04451[g]	25.13
Ba^{4+}	$5s^25p^4\ ^3P_0$	11548	11302[a]	884.8	-2.351	0.1141	0.1253[g]	8.76
Ce^{6+}	$5s^25p^4\ ^3P_0$	14697	14210[c]	703.7	-1.825	0.2159	0.2437[g]	4.63
		Se-like systems						
Zr^{6+}	$4s^24p^4\ ^3P_0$	12722	12557[d]	796.4	-1.131	0.0447	0.0468[h]	22.37
Cd^{14+}	$4s^24p^4\ ^3P_0$	28909	28828[e]	345.9	0.585	0.7612	$-$	1.31
		S-like systems						
Ge^{16+}	$3s^23p^4\ ^3P_0$	33635	33290[a]	300.4	0.228	0.2377	0.2502[h]	4.21
Kr^{20+}	$3s^23p^4\ ^3P_0$	47618	46900[a]	213.2	0.176	0.7859	0.8322[h]	1.27
Sr^{22+}	$3p^4\ ^3P_0$	50911	53400[a]	187.3	-0.160	1.2434	1.257[h]	0.805

[a] Ref. [12]; The values are compiled from the NIST database; Te-like systems [Expt.], S-like systems [Expt. or Semi.].
[b] Ref. [14]; Expt.
[c] Ref. [15]; Expt.
[d] Ref. [16]; Expt.
[e] Ref. [26]; Theor.
[f] Ref. [27]; Theor.
[g] Ref. [28]; Theor.
[h] Ref. [29]; Theor.

TABLE II. Ionization potential (IP, cm^{-1}), quadrupole moment (Θ, a.u.), and Land g-factor of the ground state.

System	State	IP Present	IP NIST	Θ	g-factor
		Te-like systems			
Te	$5p^4\ ^3P_2$	70939	72669.006(0.047)	1.22	1.467[a]
Xe^{2+}	$5s^25p^4\ ^3P_2$	247505	250400(300)	0.53	1.441
Ba^{4+}	$5s^25p^4\ ^3P_2$	475734	468000(15000)	0.32	1.424[b]
Ce^{6+}	$5s^25p^4\ ^3P_2$	748287	734000(16000)	0.19	1.407
		Se-like systems			
Zr^{6+}	$4s^24p^4\ ^3P_2$	913400	903000(16000)	0.23	1.457
Cd^{14+}	$4s^24p^4\ ^3P_2$	2894809	2887000(22000)	0.062	1.407
		S-like systems			
Ge^{16+}	$3s^23p^4\ ^3P_2$	4916400	4912400(6800)	0.042	1.445
Kr^{20+}	$3s^23p^4\ ^3P_2$	7126586	7120300(10100)	0.024	1.420
Sr^{22+}	$3p^4\ ^3P_2$	8378219	8372100(12000)	0.019	1.413

[a] Experimental value is 1.460(4) [12].
[b] The same as in our previous calculations, 1.42 [17].

Eq. (15) to solving a matrix equation (see Ref. [33] for more details).

Results for the polarizabilities of the ground and excited clock states are shown in Table III. It appears that the polarizabilities of the ground and excited clock states of all atomic systems are similar in values. This is because both clock states belong to the same fine structure manifold, and the energy intervals between them is significantly smaller than the excitation energies to the opposite-parity states (see Eq. (15)).

Some of these atomic systems have previously been studied for their polarizabilities. Review [30] and references therein have investigated the ground state polariz-

ability of Te both theoretically and experimentally, and the recommended value has been determined to be 38±4 a.u. Compared with the recommended value, our calculation (37.3 a.u.) is in excellent agreement. In our earlier work [32] a simplified approach were used leading to larger values of polarizabities of Te and Xe^{2+}; 45.96 a.u. and 47.80 a.u. for lower and upper clock states of Te, and 14.69 a.u. and 14.79 a.u. for lower and upper clock states of Xe^{2+}. These results are in reasonable agreement with our present calculations.

In our previous work [17], we calculated the polarizability of the ground and excited clock states for Ba^{4+} and found the values to be 4.4 a.u and 1.4 a.u., respec-

TABLE III. Scalar static polarizabilities of the ground and excited clock states (α_0(GS) and α_0(ES), respectively), and BBR frequency shifts for the clock transition. $\delta\nu_{\mathrm{BBR}}/\nu$ is the fractional contribution of the BBR shift, where ν is the clock transition frequency. "Total" means total scalar polarizability (core + valence). Error bars were obtained on the assumption that the accuracy for the polarizability is 10%. The last column shows the second-order Zeeman shifts, $\delta\nu_{\mathrm{SZ}}$. The notation $x[y]$ abbreviates $x \times 10^y$.

System	α_0 [a.u.] Core	α_0(GS) [a.u.] Valence	Total	α_0(ES) [a.u.] Valence	Total	$\Delta\alpha(0)$	BBR ($T = 300$ K) $\delta\nu_{\mathrm{BBR}}$ [Hz]	ν [Hz]	$\delta\nu_{\mathrm{BBR}}/\nu$	$\delta\nu_{\mathrm{SZ}}$ [Hz/(mT)^2]
					Te-like systems					
Te	8.84	28.5	37.3[a]	29.6	38.4	< 7	< 6[−2]	1.411[14]	< 4[−16]	−87
Xe^{2+}	0.835	10.1	10.9	10.4	11.2	< 2	< 2[−2]	2.437[14]	< 7[−17]	−2.02
Ba^{4+}	0.578	5.46	6.04	5.56	6.14	< 1	< 1[−2]	3.388[14]	< 3[−17]	−0.55
Ce^{6+}	0.421	3.43	3.85	3.49	3.91	< 0.6	< 5[−3]	4.260[14]	< 1[−17]	−0.22
					Se-like systems					
Zr^{6+}	0.083	1.87	1.95	1.89	1.97	< 0.1	< 1[−3]	3.764[14]	< 1[−18]	−3.72
Cd^{14+}	0.024	0.466	0.490	0.467	0.491	< 1[−2]	< 1[−5]	8.642[14]	< 1[−20]	−0.08
					S-like systems					
Ge^{16+}	0.002	0.142	0.144	0.142	0.144	< 1[−3]	< 1[−5]	9.980[14]	< 1[−20]	−0.39
Kr^{20+}	0.001	0.0812	0.0822	0.0810	0.0820	< 1[−3]	< 1[−5]	1.406[15]	< 1[−20]	−0.08
Sr^{22+}	0.063	0.0276	0.0906	0.0273	0.0903	< 1[−3]	< 1[−5]	1.601[15]	< 1[−20]	−0.04

[a] The polarizability of the Te atom has been studied before, and the recommended result is 38±4 a.u. [30].

tively. Those results are in disagreement with the present results. The reason for the disagreement comes from the fact that direct summation was used in Ref. [17]. This method works well if the summation is strongly dominated by the contribution of the low-lying states of opposite parity. This is not the case for Ba^{4+} or the other systems considered here. In this paper, we use the more accurate method described above. The accuracy of the current approach can be judged by recalling our earlier calculations [35–37]. Deviation of the calculated polarizabilities from the experimental values varies from fraction of percent for noble elements [35] to few percent for atoms with more complicated electron structure. Given also that we have excellent agreement for Te with the recommended value from literature, which has 10% uncertainty, we conclude that the accuracy of our present calculations is in the range from 1% to 10%.

Blackbody radiation (BBR) can have a significant impact on the clock transition frequency in atomic clocks. The shift in the clock transition frequency caused by BBR can be calculated as

$$\delta\nu_{\mathrm{BBR}} = -1.063 \times 10^{-12} T^4 \Delta\alpha(0), \quad (16)$$

where T is the temperature and $\Delta\alpha(0) = \alpha_0(\mathrm{ES}) - \alpha_0(\mathrm{GS})$ is the difference between the excited and ground clock-state polarizabilities. The proportionality factor here is for a shift in Hz, temperature in K, and differential polarizability in atomic units. The results of the fractional BBR shifts at room temperature are shown in Table III. It can be seen from the table that the differential polarizabilities are extremely small, which results in small values for BBR shifts. Note that even the use of the most optimistic assumption about the accuracy of the calculation of the polarizabilities (1%) leads to large uncertainties in the BBR shift. This means that the numbers for the BBR shift in Table III should be considered

as upper limits.

In order to calculate the second-order Zeeman shift ($\delta\nu_{\mathrm{SZ}}$), we have to take into account an influence caused by a weak homogeneous external magnetic field. For the determination of $\delta\nu_{\mathrm{SZ}}$, the following formula can be used [38]

$$\delta\nu_{\mathrm{SZ}} = -\frac{1}{2h}\Delta\alpha^{\mathrm{M1}}B^2, \quad (17)$$

where h is Planck's constant, B is the magnetic field, and $\Delta\alpha^{\mathrm{M1}}$ is the difference between the magnetic-dipole polarizability of the ground and excited clock states, $\Delta\alpha^{\mathrm{M1}} = \alpha^{\mathrm{M1}}(\mathrm{ES}) - \alpha^{\mathrm{M1}}(\mathrm{GS})$. The $M1$ polarizability can be calculated using Eq. (15), but the amplitude of the electric dipole transitions (A_{vn}) should be replaced with the amplitude of the magnetic dipole transitions. Our results are shown in Table III. It should be mentioned that the magnetic-dipole polarizabilities can be calculated with just a few low-lying states since their contributions dominate. In the case of the atomic systems consider here, only the first two low-lying states belonging to the same configuration give significant contributions. Here only the scalar contribution is presented. A tensor contribution of similar magnitude also exists, though it can be canceled with certain averaging schemes. In any case, the scalar results illustrate the scale of the second order Zeeman shift, which is negligibly small for small ($\sim\mu$T) magnetic fields.

D. Sensitivity of the clock transitions to variation of the fine structure constant

Variations in the fine structure constant could lead to an observable effect on the clock transition frequency. The relationship between the clock frequency and the

TABLE IV. Sensitivity of clock transitions to variation of the fine-structure constant (q, K) .

System	State	ω (cm^{-1})	q (cm^{-1})	K
		Te-like systems		
Te	$5p^4\ ^3P_0$	4706	3261	1.39
Xe^{2+}	$5s^2 5p^4\ ^3P_0$	8130	5611	1.38
Ba^{4+}	$5s^2 5p^4\ ^3P_0$	11302	5976	1.06
Ce^{6+}	$5s^2 5p^4\ ^3P_0$	14210	5907	0.83
		Se-like systems		
Zr^{6+}	$4s^2 4p^4\ ^3P_0$	12557	8939	1.42
Cd^{14+}	$4s^2 4p^4\ ^3P_0$	28828	8837	0.61
		S-like systems		
Ge^{16+}	$3s^2 3p^4\ ^3P_0$	33290	18484	1.11
Kr^{20+}	$3s^2 3p^4\ ^3P_0$	46900	17252	0.74
Sr^{22+}	$3p^4\ ^3P_0$	53400	14130	0.53

TABLE V. Lifetime-limited frequency instability for a single clock ion and the optimal logic ion based on charge-to-mass ratio (q/m); m are the average values of mass over all isotopes, taken from NIST data [12]. The notation $x[y]$ abbreviates $x \times 10^y$.

System	ν [Hz]	σ_y (1s)	Logic Ion	$\dfrac{(q/m)_{\text{Logic Ion}}}{(q/m)_{\text{Clock Ion}}}$
		Te-like systems		
Te	1.411[14]	2.6[−16]	−	−
Xe^{2+}	2.437[14]	3.4[−16]	Sr$^+$	0.749
Ba^{4+}	3.388[14]	4.1[−16]	Ca$^+$	0.857
Ce^{6+}	4.260[14]	4.5[−16]	Mg$^+$	0.961
		Se-like systems		
Zr^{6+}	3.764[14]	2.3[−16]	Be$^+$	1.687
Cd^{14+}	8.642[14]	4.2[−16]	Be$^+$	0.891
		S-like systems		
Ge^{16+}	9.980[14]	2.0[−16]	Be$^+$	0.504
Kr^{20+}	1.406[15]	2.6[−16]	Be$^+$	0.465
Sr^{22+}	1.601[15]	2.9[−16]	Be$^+$	0.442

fine-structure constant in the vicinity of their physical values can be expressed as:

$$\omega = \omega_0 + q\left[\left(\frac{\alpha}{\alpha_0}\right)^2 - 1\right], \qquad (18)$$

where α_0 and ω_0 are the laboratory values of the fine structure constant and the transition frequency, respectively, and q is the sensitivity coefficient that is determined from atomic calculations [39]. Note that we do not consider variation of atomic unit of energy $m_e e^4/\hbar^2$ since it cancels out in the ratio of frequencies. Variation of dimensionfull parameters like $m_e e^4/\hbar^2$ depend on the units one uses. For example, in atomic units it is equal to one and does not vary. Therefore, dependence of frequencies on α appears due to relativistic corrections.

The change in a frequency ratio ω_1/ω_2 caused by a change in α is

$$\delta\left(\frac{\omega_1}{\omega_2}\right) = \frac{\delta\omega_1}{\omega_1} - \frac{\delta\omega_2}{\omega_2} = (K_1 - K_2)\frac{\delta\alpha}{\alpha}. \qquad (19)$$

The value $K = 2q/\omega$ is often called the enhancement factor. We calculate q and K by using two different values of α and calculating the numerical derivative

$$q = \frac{\omega(x) - \omega(-x)}{2x}, \qquad (20)$$

where $x = (\alpha/\alpha_0)^2 - 1$ [see Eq. (18)]. In order to achieve linear behaviour, the x value must be small; however, it must be large enough to suppress numerical noise. Accurate results can be obtained by using $x = 0.01$. A summary of the calculated values of q and K is given in Table IV.

IV. EXPERIMENTAL OUTLOOK

Here, we discuss the experimental outlook for the development of optical atomic clocks based on these sys-

tems. The systematic shifts considered in previous sections are limited by the atomic properties of the respective system. However, when estimating the expected clock performance, it is important to also consider systematic shifts due to ion motion (time dilation) and the expected frequency instability. To estimate the frequency instability, we consider a Ramsey interrogation sequence for a single ion with interrogation time equal to the natural lifetime, assuming the instability to be limited by fundamental quantum projection noise [40]. Under these conditions, the fractional instability is given by [10, 41]

$$\sigma_y(t) = \frac{0.412}{\nu\sqrt{\tau t}}, \qquad (21)$$

where ν is the clock frequency, τ is the lifetime of the excited clock state, and t is the averaging time. These results are summarized in Table V. All systems exhibit frequency instabilities, for a single clock ion, of $\sigma_y(t) < 5 \times 10^{-16}/\sqrt{t/s}$. This level of performance is comparable to recent demonstrations in Al$^+$ and Yb$^+$ [3, 42, 43].

Since none of the ions proposed here possess electric dipole-allowed ($E1$) transitions for cooling and state readout, it will be necessary to utilize a scheme such as quantum-logic spectroscopy (QLS) for clock operations [44]. The application of QLS requires the clock ion to be co-trapped with an auxiliary readout "logic" ion which does possess a laser-accessible transition for cooling and state readout operations. In addition, ion-based optical clocks are susceptible to time-dilation shifts due to driven excess micromotion (EMM) and secular (thermal) motion due to the finite ion temperature. The secular motion can be reduced by applying sympathetic cooling of the clock ion via the co-trapped logic ion. The most efficient sympathetic cooling occurs when the charge-to-mass ratio of the clock ion is equal to that of the logic ion [45]. For each ion considered here, we estimate the logic ion which would be the best match for sympathetic

cooling. These results are listed in Table V.

The excess micromotion shift is a result of imperfections in the trap potential, typically caused by stray electric fields and/or phase shifts between rf drive electrodes that lead to residual rf fields at the location of the ion [18]. This shift can be minimized by using a trap design which has been shown to have low EMM [3, 46].

V. SUMMARY

In conclusion, we identify group 16-like ions as promising candidates for high-accuracy optical clocks. This class of ions exhibit irregular ordering in the ground ^3P_J fine structure manifold for large enough ionization degree, leading to $E2$ clock transitions with narrow natural linewidths. Due to the increased charge state, several common systematic shifts are reduced compared to many of the current species used for optical clocks.

ACKNOWLEDGMENTS

[1] A. D. Ludlow *et al.*, Optical atomic clocks, Rev. Mod. Phys. **87**, 637 (2015).

[2] M. S. Safronova *et al.*, Search for new physics with atoms and molecules, Rev. Mod. Phys. **90**, 025008 (2018).

[3] S. M. Brewer *et al.*, Phys. Rev. Lett. **123**, 033201 (2019).

[4] W. F. McGrew *et al.*, Atomic clock performance enabling geodesy below the centimetre level, Nature **564**, 87 (2018).

[5] T. Bothwell, D. Kedar, E. Oelker, J. M. Robinson, S. L. Bromley, W. L. Tew, J. Ye, and C. J. Kennedy, JILA SrI optical lattice clock with uncertainty of 2.0×10^{-18}, Metrologia **56**, 065004 (2019).

[6] N. Huntemann *et al.*, Single-ion atomic clock with 3×10^{-18} systematic uncertainty, Phys. Rev. Lett. **116**, 063001 (2016).

[7] J. C. Berengut, V. A. Dzuba, and V. V. Flambaum, Enhanced laboratory sensitivity to variation of the fine structure constant using highly-charged ions, Phys. Rev. Lett. **105**, 120801 (2010).

[8] J. C. Berengut, V. A. Dzuba, V. V. Flambaum, and A. Ong, Electron-hole transitions in multiply-charged ions for precision laser spectroscopy and searching for alpha-variation, Phys. Rev. Lett. **106**, 210802 (2011).

[9] J. C. Berengut, V. A. Dzuba, V. V. Flambaum, and A. Ong, Optical transitions in highly-charged californium ions with high sensitivity to variation of the fine-structure constant, Phys. Rev. Lett. **109**, 070802 (2012).

[10] M. G. Kozlov, M. S. Safronova, J. R. Crespo López-Urrutia, and P. O. Schmidt, Highly charged ions: Optical clocks and applications in fundamental physics, Rev. Mod. Phys. **90**, 045005 (2018).

[11] J. C. Berengut, V. A. Dzuba, V. V. Flambaum, and A. Ong, Highly charged ions with e1, m1, and e2 transitions within laser range, Phys. Rev. A **86**, 022517 (2012).

[12] A. Kramida, Y. Ralchenko, J. Reader, and N. A. Team, (2020), NIST Atomic Spectra Database (ver. 5.7.1), [Online]. Available: https://physics.nist.gov/asd [2020, September 26]. National Institute of Standards and Technology, Gaithersburg, MD. DOI: https://doi.org/10.18434/T4W30F.

[13] K. Cheng, Y.-K. Kim, and J. Desclaux, Electric dipole, quadrupole, and magnetic dipole transition probabilities of ions isoelectronic to the first-row atoms, li through f, Atomic Data and Nuclear Data Tables **24**, 111 (1979).

[14] R. Gayasov, Y. N. Joshi, and A. Tauheed, Sixth spectrum of lanthanum (la vi): analysis of the $5s^25p^4$, $5s5p^5$ and $5s^25p^3(5d + 6s)$ configurations, J. Phys. B: At. Mol. Opt. Phys. **30**, 873 (1997).

[15] A. Tauheed and Y. N. Joshi, The $5s^25p^4$-($5s5p^5 + 5p^36s$) transitions in ce vii and $5s^25p^3$ ^4s - $5s5p^4$ ^4p transitions in ce viii, Can. J. Phys. **86**, 713 (2008).

[16] J. Reader and N. Acquista, $4s^24p^4$-$4s4p^5$ transitions in zr vii, nb viii, and mo ix, J. Opt. Soc. Am. **66**, 896 (1976).

[17] K. Beloy, V. A. Dzuba, and S. M. Brewer, Quadruply ionized barium as a candidate for a high-accuracy optical clock, Phys. Rev. Lett. **125**, 173002 (2020).

[18] D. J. Berkeland *et al.*, Minimization of ion micromotion in a paul trap, J. Appl. Phys. **83**, 5025 (1998).

[19] V. A. Dzuba, Combination of the single-double–coupled-cluster and the configuration-interaction methods: Application to barium, lutetium, and their ions, Phys. Rev. A **90**, 012517 (2014).

[20] W. R. Johnson and J. Sapirstein, Computation of second-order many-body corrections in relativistic atomic systems, Phys. Rev. Lett. **57**, 1126 (1986).

[21] W. R. Johnson, S. A. Blundell, and J. Sapirstein, Finite basis sets for the dirac equation constructed from b splines, Phys. Rev. A **37**, 307 (1988).

[22] V. A. Dzuba, V. V. Flambaum, P. G. Silvestrov, and O. P. Sushkov, Correlation potential method for the calculation of energy levels, hyperfine structure and e1 transition amplitudes in atoms with one unpaired electron, J. Phys. B: *At. Mol. Phys.* **20**, 1399 (1987).

[23] V. A. Dzuba, V. V. Flambaum, and M. G. Kozlov, Combination of the many-body perturbation theory with the configuration interaction method, Phys. Rev. A **54**, 3948 (1996).

[24] V. A. Dzuba, J. C. Berengut, C. Harabati, and V. V. Flambaum, Combining configuration interaction with perturbation theory for atoms with a large number of

valence electrons, Phys. Rev. A **95**, 012503 (2017).

[25] V. A. Dzuba, V. V. Flambaum, P. G. Silvestrov, and O. P. Sushkov, Correlation potential method for the calculation of energy levels, hyperfine structure and e1 transition amplitudes in atoms with one unpaired electron, Journal of Physics B: Atomic and Molecular Physics **20**, 1399 (1987).

[26] K. Wang, X. Yang, Z. Chen, R. Si, C. Chen, J. Yan, X. H. Zhao, and W. Dang, Energy levels, lifetimes, and transition rates for the selenium isoelectronic sequence pd xiii−te xix, xe xxi−nd xxvii, w xli, At Data Nucl Data Tables **117**, 1 (2017).

[27] R. H. Garstang, Transition probabilities of forbidden lines, J. Res. Natl. Bur. Stand. A Phys. Chem. **68**, 61 (1964).

[28] E. Bimont, J. E. Hansen, P. Quinet, and C. J. Zeippen, Forbidden transitions of astrophysical interest in the $5p^k$ (k= 1-5) configurations, Astron. Astrophys., Suppl. Ser. **111**, 333 (1995).

[29] E. Bimont and J. E. Hansen, Forbidden transitions in $3p^4$ and $4p^4$ configurations, Phys. Scr. **34**, 116 (1986).

[30] P. Schwerdtfegera and J. K. Nagle, 2018 table of static dipole polarizabilities of theneutral elements in the periodic table, Molecular Physics **117**, 1200 (2019).

[31] W. Itano, External-field shifts of the ^{199}hg$^+$ optical frequency standard, J. Res. Natl. Inst. Stand. Technol. **105**, 829 (2000).

[32] A. Kozlov, V. A. Dzuba, and V. V. Flambaum, Optical atomic clocks with suppressed blackbody-radiation shift, Phys. Rev. A **90**, 042505 (2014).

[33] V. Dzuba, Calculation of polarizabilities for atoms with open shells, Symmetry **12**, 1950 (2020).

[34] A. Dalgarno and J. T. Lewis, The exact calculation of longrange forces between atoms by perturbation theory, Proc. R. Soc. London A **233**, 70 (1955).

[35] V. A. Dzuba, V. V. Flambaum, J. S. M. Ginges, and M. G. Kozlov, Electric dipole moments of hg, xe, rn, ra, pu, and tlf induced by the nuclear schiff moment and limits on time-reversal violating interactions, Phys. Rev. A **66**, 012111 (2002).

[36] V. A. Dzuba and V. V. Flambaum, Calculation of the (t , p)-odd electric dipole moment of thallium and cesium, Phys. Rev. A **80**, 062509 (2009).

[37] V. A. Dzuba and A. Derevianko, Dynamic polarizabilities and related properties of clock states of the ytterbium atom, J. Phys. B **43**, 074011 (2010).

[38] S. G. Porsev and M. S. Safronova, Calculation of higher-order corrections to the light shift of the $5s^2$ $^1S_0 - 5s5p$ $^3P_0^o$ clock transition in cd, Phys. Rev. A **102**, 012811 (2020).

[39] V. V. Flambaum and V. A. Dzuba, Search for variation of the fundamental constants in atomic, molecular, and nuclear spectra, Can. J. Phys. **87**, 25 (2009).

[40] W. M. Itano *et al.*, Quantum projection noise: Pupulation flucturation in two-level systems, Phys. Rev. A **47**, 3554 (1993).

[41] E. Peik, T. Schneider, and C. Tamm, Laser frequency stabilization to a single ion, J. Phys. B **39**, 145 (2005).

[42] E. R. Clements *et al.*, Lifetime-limited interrogation of two independent ^{27}al$^+$ clocks using correlation spectroscopy, Phys. Rev. Lett. **125**, 243602 (2020).

[43] C. Sanner, N. Huntemann, R. Lange, C. Tamm, E. Peik, M. S. Safronova, and S. G. Porsev, Optical clock comparison for lorentz symmetry testing, Nature **567**, 204 (2019).

[44] P. O. Schmidt *et al.*, Spectroscopy using quantum logic, Science **309**, 749 (2005).

[45] J. B. Wübbena, S. Amairi, O. Mandel, and P. O. Schmidt, Sympathetic cooling of mixed-species two-ion crystals for precision spectroscopy, Phys. Rev. A **85**, 043412 (2012).

[46] K. Pyka, N. Herschbach, J. Keller, and T. E. Mehlstäubler, A high-precision segmented paul trap with minimized micromotioin for an optical multiple-ion clock, Appl. Phys. B **114**, 231 (2013).

[47] (2010), katana (shared computational cluster), [https://doi.org/10.26190/669x-a286] University of New South Wales, Sydney.